nature physics

SUPPLEMENTARY INFORMATION

https://doi.org/10.1038/s41567-018-0270-1

In the format provided by the authors and unedited.

Driven-dissipative non-equilibrium Bose–Einstein condensation of less than ten photons

Benjamin T. Walker[1,2], Lucas C. Flatten[3], Henry J. Hesten[1,2], Florian Mintert[1], David Hunger[4], Aurélien A. P. Trichet[3], Jason M. Smith[3] and Robert A. Nyman[1]*

[1]Quantum Optics and Laser Science group, Blackett Laboratory, Imperial College, London, UK. [2]Centre for Doctoral Training in Controlled Quantum Dynamics, Imperial College, London, UK. [3]Department of Materials, University of Oxford, Oxford, UK. [4]Physikalisches Institut, Karlsruher Institut für Technologie, Karlsruhe, Germany. *e-mail: r.nyman@imperial.ac.uk

Driven-dissipative non-equilibrium Bose-Einstein condensation of less than 10 photons: Supplementary material

Benjamin T. Walker,[1,2] Lucas C. Flatten,[3] Henry J. Hesten,[1,2] Florian Mintert,[1]
David Hunger,[4] Aurélien A. P. Trichet,[3] Jason M. Smith,[3] and Robert A. Nyman[1,*]

[1] *Quantum Optics and Laser Science group, Blackett Laboratory, Imperial College London, Prince Consort Road, SW7 2AZ, UK*
[2] *Centre for Doctoral Training in Controlled Quantum Dynamics, Imperial College London, Prince Consort Road, SW7 2AZ, UK*
[3] *Department of Materials, University of Oxford, Parks Road, Oxford, OX1 3PH, UK*
[4] *Physikalisches Institut, Karlsruher Institut für Technologie, Wolfgang-Gaede-Straße 1, 76131 Karlsruhe, Germany*

(Dated: Friday 6th July, 2018)

This document is intended as supplementary material, to be read alongside the Main Text.

MIRROR FABRICATION

FIB milling makes nanometric precision of surface topography possible over a large range of feature sizes and radii of curvature. After the FIB milling, the surface of the concave feature was treated with a CO_2 laser to melt a thin layer of material and achieve a lower surface roughness upon resolidification [1]. Surface roughness was measured to be 0.3 nm (rms) after the smoothing step. See Fig. 1(a), where the right two columns were treated with the CO_2 laser and the left columns untreated.

To verify the optical quality of the concave surface the decay of the photon population of a longitudinal cavity mode after a short (≈ 6 ps) populating pulse was probed and finesses of $2\text{–}5 \times 10^4$ were found, varying from feature to feature. At the 10th longitudinal cavity mode this finesse corresponds to a cavity lifetime of up to 150 ps. The nominal transmission and absorption for each dielectric mirror are 30 ppm and 10 ppm respectively, at 577 nm (free space wavelength), totalling 80 ppm of coating-induced losses per round trip. The losses are consistent with the known surface roughness. These finesse measurements used an air gap. With ethylene glycol of refractive index 1.44 one would expect finesse less than 1×10^4 due to enhanced scattering from the rough surface at shorter wavelength and decreased reflection from the front surface of the dielectric stack. The measured cavity lifetime as discussed in Main Text, Fig. 4 (bottom panel) is just 5 ps. The unaccounted-for losses are most likely due to a combination of chemical impurities in dye and solvent, dye aggregation at high concentrations, and dirt and mechanical damage due to handling mirrors in a standard laboratory rather than a clean room.

The mirrors permit us to reach harmonic trapping frequencies, equivalent to the transverse mode spacing of the optical microcavity, up to $f = 1.7$ THz, or $0.25 \times k_B T$ where T is room temperature, depending on the mirror RoC and cavity length. When hf is of order $k_B T$ finite-size effects become important and the critical photon number for BEC is small. The depth of features is greater than one complete longitudinal free-spectral range. That implies an effective trap depth of greater than $h\times 60$ THz or 10 $k_B T$, meaning that more than 99.95% of thermal photons are trapped.

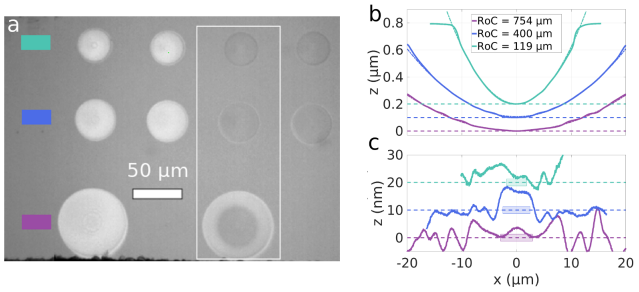

FIG. 1. Microfabrication. (a) A white-light microscope image of the mirrors used. (b) Quantitative analysis shows parabolae, and we have used the features with effective radii of curvature 400 µm. Colours indicate from which row the features are plotted. The white box indicates the column. Features left of the column of (a) are not laser smoothed; figures in the box and to the right have been smoothed. (c) Deviations of mirror profile (continuous line) from hemispherical model (dashed line), stacked vertically for better visibility. The length of the shaded bars corresponds to the ground state mode waist on the curved mirror. The surface roughness is as low as 0.3 nm.

It is important to note that the light penetrates the mirrors by an effective number q_0 of half-wavelengths. If the true longitudinal mode number (given by the product of cavity round trip time and light frequency) is q, then the open length of the cavity is $(q - q_0)\lambda^*/2$ where λ^* is the wavelength of light in the medium. It is this latter length which enters into calculations for trapping frequency [2]. Also, the effective number density of molecules must be re-normalised by a factor $(q - q_0)/q$ (see below).

A COMPLETE MODEL FOR DYE-MICROCAVITY PHOTONS

In this section we describe the full non-equilibrium model which we compare to the data in the Main Text, and how we ascertain the appropriate microscopic parameters.

The assumption that all photon modes couple equally to all molecules as used in the simplified model of Eqns. (3)–(6) in the Main Text is not valid for many of our experimental parameters. Instead, we make use of the updated model of Ref. [3] which takes into account both position-dependent coupling to spatially-varying cavity photon modes and an inhomogeneous excited-state fraction of the dye molecules. Some of us (HJH, RAN and FM) have used precisely this model to describe the phase diagram of multimode photon condensates [4]. We have reached a good quantitative comparison between the experimental data and the model by fixing as many parameters as possible. Here, we justify the values of the remaining parameters.

The first parameter to be set is the cavity loss rate, κ. From the coherence measurements, in the Main Text Fig. 4 (lower panel), we know that $1/\kappa = 5.2 \pm 0.8$ ps. We fix the value at 5 ps for the remainder of this work unless otherwise stated.

Light-matter coupling strength

The next parameter to fix is the light-matter coupling strength, $\Gamma(\pm\delta)$. The formalism is stated explicitly in the above-mentioned articles, especially Ref. [4], Eqns. (1)–(3). We note that $\Gamma(\delta)$ is converted to a rate by being multiplied by the molecular density. The correct density ρ to use for our near-planar microcavities is the areal density of molecules, which itself is the bulk molecular concentration multiplied by the length between the mirrors. The molecular concentration is 2.4 mM, giving molecular number density $n_{mol} = 1.4 \times 10^{24}\mathrm{m}^{-3}$. Since the light penetrates the dielectric mirrors, for a cavity of longitudinal mode number q, this between-mirror length is about $L_0 = (q - q_0)\lambda^*/2$ where $q_0 \sim 4$ and λ^* is the wavelength of light in the medium. In this work we set $q = 8$, and for simplicity we keep $\lambda^* = 400$ nm (equivalent to about 570 nm in free space). Thus $L_0 = 800$ nm, and $\rho = n_{mol}L_0$. The re-absorption rate for a bulk system with in-medium speed of light c^* is $n_{mol}c^*\sigma(\lambda)$ for a measured wavelength-dependent light-scattering cross section $\sigma(\lambda)$. Hence, $n_{mol}\sigma(\lambda)c* = \rho\Gamma(\delta) \Rightarrow \Gamma(\delta) = \sigma(\lambda)c*/L_0$. In the Main Text, the discussion of molecular density uses, for simplicity, the effective concentration of dye molecules taking into account the optical path within the dielectric, written as $\overline{n}_{mol} = n_{mol}(q - q_0)/q$. Finally, conversion between lab-optimised wavelengths λ and simulation-optimised detunings δ is via the definition of a zero-phonon line where $\delta = 0$, so that $\Gamma(\delta) = \Gamma(-\delta)$, i.e. the peak-normalised absorption and emission spectra cross, which is at 545 nm (see [5]).

Molecular decay rate

To match the depth and breadth of the threshold phenomenon in population as a function of pump rate or power, adjusting the fraction of spontaneous molecular de-excitation that goes into creating cavity photons is the most logical step. This fraction is known as the β parameter of microlaser physics. Since the intracavity emission is fixed, the only parameter in the model which can set β is $\Gamma_\downarrow$, which is expected to be dominated by spontaneous emission into free space. The bulk rate is $\Gamma_\downarrow^{bulk} = 0.25$ ns^{-1}. Numerical experiments show $\Gamma_\downarrow = 0.03$ ns^{-1} gives a much more appropriate match to the data. We conclude that spontaneous emission into free space is strongly suppressed by the simple fact that the mirrors subtend a very large solid angle at the centre of the cavity. The mirrors also have a rather broad stop band and a wide angle over which their transmission is very low. Hereafter, and in the Main Text, we fix $\Gamma_\downarrow = 0.03$ ns^{-1}.

Pump-spot size

The only remaining adjustable parameter is the pump spot size. Experimentally, we focus the spot as small as possible, given the numerical aperture available. The lower diffraction limit for our optics is between 1.3 μm (the diameter of the first zero of the focal Airy disk assuming a uniform beam filling our focussing lens) and 1.7 μm (based on Gaussian optics for our roughly-Gaussian pump beam). In our simulation, the value is encoded in harmonic oscillator lengths, $l_{ho} = 1.2$ μm for 1.7 THz harmonic-oscillator mode spacing. In the simulation, we assume an elliptical spot, whose major axis is $\sqrt{2}$ times larger than its minor axis, since the beam is incident on the cavity at approximately 45° to pass through the dielectric mirror efficiently. From one experimental run to the next the pump spot may be re-aligned and refocused to the smallest achievable spot size, with precision roughly equivalent to the depth of focus, i.e. we reliably achieve spot sizes of 1–2l_{ho}. We focus as small as possible to minimise pumping highly-excited transverse modes of an secondary longitudinal mode of the cavity. We detect those modes in experimental spectra, and can pass lasing threshold if we do not carefully align and focus our pump beam.

In Fig. 2 we see results of a simulation of thermalisation of light (far below threshold pump rate). The parameters are as described above, but we vary both cavity cutoff wavelength and pump spot size, for three possible cavity lifetimes. The Boltzmann distribution is then fitted to the mode populations and an effective temperature extracted. For the longest cavity lifetimes, there is a substantial region (large pump spot, 560–580 nm cutoff)

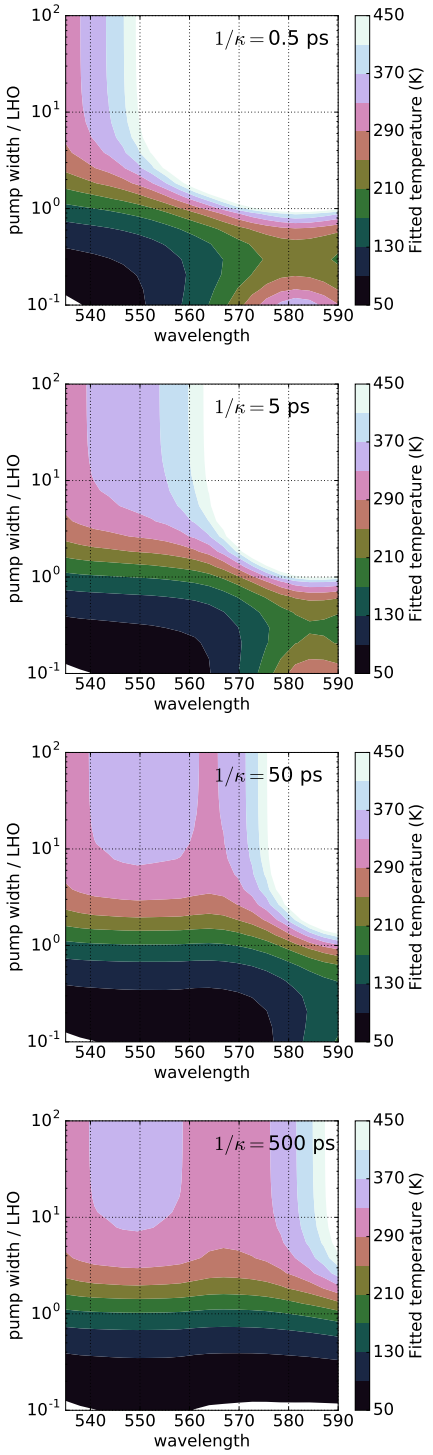

FIG. 2. Effective temperature (see side bar for scale) derived by fitting simulated mode populations far below threshold pump rate, as a function of pump spot size and cavity cutoff wavelength. The inverse of the spontaneous emission lifetime is set to $1/\Gamma_\downarrow = 32$ ns as determined from the width of the threshold feature. Top to bottom, the cavity lifetime is increased.

over which the temperature matches room temperature, independent of the precise parameter values. This represents true thermal equilibrium, and requires at least 20 re-absorption events per cavity loss. As the cavity lifetime is reduced, the region covers a smaller range of cutoff wavelengths, and even disappears for the lifetimes we believe describe our experiments, 5 ps. For that lowest lifetime, there is no true thermal equilibrium but the re-absorption and emission events have significantly redistributed the cavity light from the emission spectrum of the dye towards the thermal equilibrium distribution. In the Main Text, Fig. 1(c) we find effective temperatures of 150 ± 20 K for 560 nm cutoff wavelength, suggesting pump spot very close to the diffraction limit, around 1 l_{ho}. Our experiment therefore is in a non-equilibrium regime (in contrast to say Ref. [6]), but nonetheless a near-equilibrium description with an adjustable effective temperature is appropriate.

The simulations here and in the Main Text are run using a total of 15 modes across 5 non-degenerate energy levels. We have run example simulations using 28 modes over 7 levels, and found no significant differences in the results.

NON-EQUILIBRIUM DEFINITIONS OF CONDENSATION

There is no unique recipe for determining the threshold for condensation, especially in finite-sized systems and non-equilibrium. A common starting point is the Penrose-Onsager criterion [7] which can be interpreted as stating that condensation occurs when the occupation of a mode of the multi-particle system has an occupancy which grows linearly with the total number of particles in the system. They call this specifically *Bose-Einstein* condensation. Their definition does not strictly distinguish what we are labelling as single-mode Bose-Einstein condensation from multimode condensation. It also cannot be trivially mapped onto finite-sized systems as the notion of extensivity is only valid in the thermodynamic limit.

Let us now review several alternative operational definitions of threshold from a variety of physical implementations (laser physics, atomic gases, general statistical physics) with the aim of applying them to our finite-size, non-equilibrium system with multiple modes and variable total particle number, which is capable of showing multimode condensation.

A. Generalised condensation in a specific mode labelled i occurs when the number of particles in that mode n_i is a finite and constant fraction of the total particle number n_{tot}, but the populations in non-condensed (or depleted) modes are not proportional, as the total particle number goes to infinity: $\lim_{n_{tot}\to\infty} n_i/n_{tot} =$

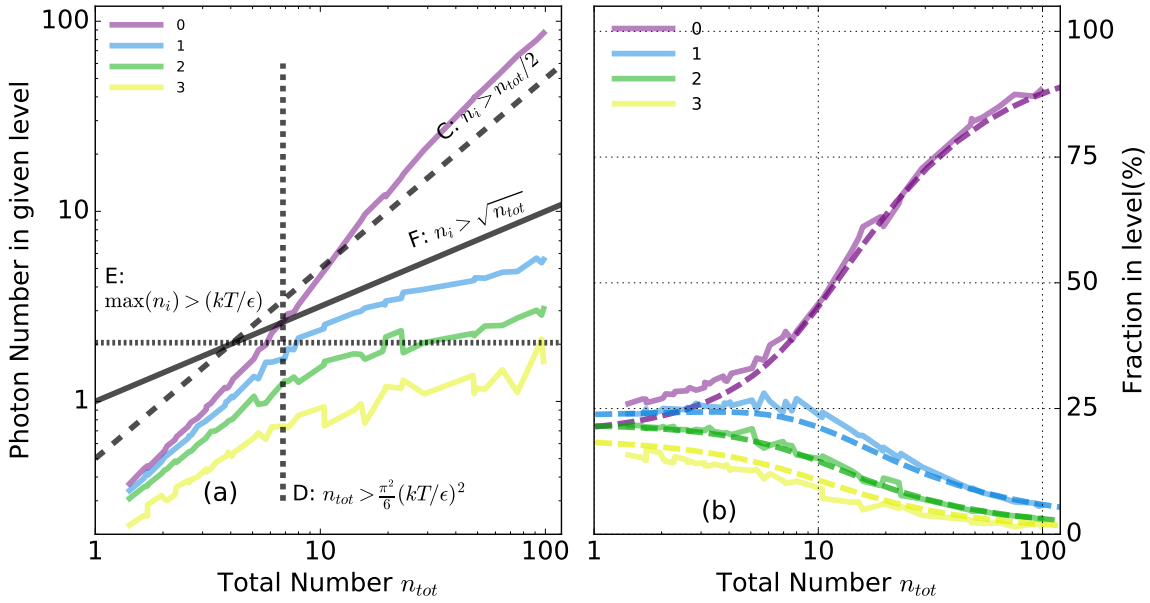

FIG. 3. Criteria for determining the condensation threshold: see text for descriptions. Criteria A. and B. dot not allow us to determine threshold, and G. is not relevant to our multi-mode system. Left panel: number in each mode as a function of total photon number, together with labelled criteria. A temperature fit of 150 K was used, with energy level spacing $h\times1.7$ THz. Right panel: the same data, as a fraction, showing clearly that an increasing fraction of photons go into the ground mode for increasing photon number. The non-equilibrium model results are shown as dashed lines.

$\mathcal{O}(1)$. This criterion is discussed in Ref. [8] in a very general context and holds for both Bose-Einstein and multimode condensation, regardless of notions of thermal equilibrium. While it makes clear whether condensation happens or not, because it is only applicable in the asymptotic limit of large particle number, a well-defined threshold criterion cannot be derived from it.

B. A linear-growth condition for BEC is when criterion A. holds for one and only one mode $i = 0$, that being the lowest energy mode. This holds for non-equilibrium systems but only in the asymptotic limit of large n_{tot} and so cannot be used to determine threshold. This is a specialised version of and is used in, for example, Ref. [9].

C. If more than half of all particles are in one state, then that must be the only condensed state. If that mode is the lowest energy mode, one can then say that the mode is Bose-Einstein condensed. Since it holds in a finite system it can be used to define threshold: $n_i/n_{tot} > 1/2$. Criteria A. and B. are necessary but not sufficient conditions for this criterion; this is a very strict criterion, used by Ref. [10].

D. In trapped, conservative, thermal-equilibrium Bose gases (e.g. cold atomic vapours) BEC is considered to occur when $n_{tot} > \lim_{n_{tot}->\infty} n_{tot} - n_0$, i.e. the total population exceeds the saturated excited-mode population in the infinite particle-number limit [11]. For simple trapping potentials this limit can be calculated analytically. For example, in a 2D trap of angular frequency Ω and energy $\hbar\Omega = \epsilon$, relevant to our experiments, this criterion becomes $n_{tot} > \left(\pi^2/6\right)\left(k_BT/\epsilon\right)^2$, for one polarisation state. This criterion is valid only for thermal equilibrium in a well-known potential energy landscape.

E. In criterion D., at threshold the ground state population is well defined. To leading order one finds $n_0 > k_BT/\epsilon$ [12] as an alternative criterion suitable for finite-sized systems. Despite being derived from equilibrium considerations, Kirton and Keeling [12] use it even away from equilibrium, with generalised condensation occuring when at least one mode (not necessarily the ground mode) has this population.

F. A consequence of the same analysis is $n_0 = n_{tot}^{1/\alpha}$ at the threshold, with $\alpha > 1$ being the dimensionality. For our system, $\alpha = 2$ so we find a criterion of $n_0 > \sqrt{n_{tot}}$ [11, 12]. While this is strictly an equilibrium criterion, it still makes sense out of equilibrium, generalised to $n_i > \sqrt{n_{tot}}$. When there are few particles, few modes may condense. With many particles, many, even all, modes may condense. This $\mathcal{O}(n^{1/2})$ criterion neatly separates saturated or depleted states with $n_i = \mathcal{O}(n^0)$ from condensed modes where $n_i = \mathcal{O}(n^1)$.

G. Mode occupancy of one, $n_i > 1$, is considered a threshold for microlasers by some authors (e.g.

Ref. [13]). This is a non-equilibrium condition but based on a single mode. We consider condensation (as opposed to lasing) to be a phenomenon which occurs in multi-mode systems, this criterion is not useful to us here, except in comparison to the microlaser model of Main Text, Eqn. (10).

It is possible to invent other *ad hoc* criteria for threshold, but robust criteria which can be applied in the presence of experimental noise are not obvious.

In Fig. 3 we see the same data as in the Main Text Fig. 1(c). We determine threshold by comparison with the criteria listed here. Only criteria D. and E. make use of the temperature extracted from the fits to the Bose-Einstein distribution. If the criteria all represented the same physical interpretation of threshold, we would expect them to pass through one unique point. They do not, implying that the criteria are logically distinct. Despite the system being out of equilibrium, the two equilibrium criteria D. and E. (applied with $T = 150\ K$ as fitted) coincide closely with the data to within experimental noise. Criterion F. almost coincides. The coincidence of all three criteria bracket the data, at a total photon number of 7 ± 1 with $\sqrt{7}$ photons in the ground state. This is the figure we state for threshold in the Main Text. Only C. gives a significantly different value of threshold, at around 11 photons. We consider this latter criterion overly strict for establishing BEC unless there is some ambiguity which the other criteria cannot be used to resolve.

Despite the imperfect saturation of excited states due to the deviation from thermal equilibrium, according to criterion F., only the ground state goes above threshold within the range of data taken here. All other modes remain below threshold or depleted. The most common operational concept of BEC as large-scale occupation of the ground state alone is then clearly applicable to our system, despite its finite size and imperfect equilibration.

FITTING THE BOSE-EINSTEIN AND MICROLASER DISTRIBUTIONS AND CALIBRATING PHOTON NUMBER

To extract a temperature we fit the Bose-Einstein distribution to the data, as shown in the Main Text, Fig. 1(c). The procedure is a hierarchical least-squares fit using log-spaced residuals to account for the large dynamical range of the data. The function fitted is the Bose-Einstein distribution, summed over the first five lowest energy levels (15 modes). In an outer optimisation covering the complete data set to be fitted, the temperature T and a number calibration scale N are selected. In an inner loop, for each total particle number, the chemical potential is varied to minimise the residuals between the data and the distribution across the 5 modes, using the specified value of T. The temperature T and calibration N are varied to globally minimise the total residuals. Not all data are used for the fit. Far above threshold, the excited state populations do not saturate which introduces a bias to the fitted temperature, so we truncate the above-threshold data when fitting. Varying the truncation point varies the temperature by approximately 20 K, hence we quote 150 ± 20 K for the fitted temperature.

To fit the microlaser distribution, Main Text, Eqn. (10), we fit to the ground mode population alone, as a function of pump power. There are three parameters: the spontaneous emission fraction β, the number calibration N and a scaling G between nominal pump laser power and the pump rate of the molecules in units of the cavity lifetime. This latter parameter is of no fundamental importance.

We calibrate the spectrometer with a known pump power laser beam, but the coupling from intra-cavity photons to the spectrometer detection is uncertain, hence the need for the number calibration parameter N in the fits. The fits to the two different distributions yield similar calibration values, of approximately 3.5, implying that there we have unaccounted-for but not-unreasonable losses of about 70% of our light between cavity and detector. A large part of the difference may come from the mirror transmission, for which we use the manufacturer's calculated specification interpolated to our required wavelengths rather than a direct measurement. In practice, having used fitting to check the value of N, we fix one value and then re-fit both models.

POLARISATION STATES

In the thermal equilibrium model we take the degeneracy of the ith excited level to be $i+1$ as appropriate for a symmetric 2D harmonic oscillator potential. In doing so, we assume that there is only one polarisation mode for the light. In reality there are two. These two polarisations introduce an ambiguity to the experimental observation of threshold: if one mode condenses but not the other, how could we tell without polarisation-sensitive detection?

The polarisation of photon BECs has only very recently been studied theoretically [14] and experimentally [15]. The main conclusion of the theoretical modelling is that the polarisation degree of freedom thermalises through rotational diffusion of the dye molecules, which is a much slower process than the energetic or spatial thermalisation. The experiments show that while the BEC (the ground state when condensed) is mostly linearly polarised along the pump axis, the other modes remain unpolarised. This evidence suggests that the two polarisation degrees of freedom interact only weakly with each other, especially in our system with a rather short

cavity lifetime (5 ps) compared to the rotation diffusion time constant (about 2 ns).

In our experiments we place a polarising filter in front of the spectrometer used for detection, aligned to maximise transmission above threshold photon number. Since the unobserved, orthogonal polarisation component does not interact with the observed component, we simply make the assumption that the polarisation degeneracy is unity for our calculations. This is standard practice in photon BEC for measuring, for example, photon-photon correlations [16] or coherence [6, 17].

* Correspondence to r.nyman@imperial.ac.uk

[1] Hunger, D., Deutsch, C., Barbour, R. J., Warburton, R. J. & Reichel, J. Laser micro-fabrication of concave, low-roughness features in silica. *AIP Advances* **2**, 012119 (2012).

[2] Marelic, J., Walker, B. T. & Nyman, R. A. Phase-space views into dye-microcavity thermalized and condensed photons. *Phys. Rev. A* **94**, 063812 (2016).

[3] Keeling, J. & Kirton, P. Spatial dynamics, thermalization, and gain clamping in a photon condensate. *Phys. Rev. A* **93**, 013829 (2016).

[4] Hesten, H. J., Nyman, R. A. & Mintert, F. Decondensation in non-equilibrium photonic condensates: when less is more. *Phys. Rev. Lett* **120**, 040601 (2018).

[5] Nyman, R. A. Absorption and Fluorescence spectra of Rhodamine 6G (2017). `http://dx.doi.org/10.5281/zenodo.569817`.

[6] Damm, T., Dung, D., Vewinger, F., Weitz, M. & Schmitt, J. First-order spatial coherence measurements in a thermalized two-dimensional photonic quantum gas. *Nature Communications* **8**, 158 (2017).

[7] Penrose, O. & Onsager, L. Bose-Einstein Condensation and Liquid Helium. *Phys. Rev.* **104**, 576–584 (1956).

[8] Knebel, J., Weber, M. F., Krüger, T. & Frey, E. Evolutionary games of condensates in coupled birth–death processes. *Nature communications* **6**, 6977 (2015).

[9] Vorberg, D., Wustmann, W., Ketzmerick, R. & Eckardt, A. Generalized Bose-Einstein Condensation into Multiple States in Driven-Dissipative Systems. *Phys. Rev. Lett.* **111**, 240405 (2013).

[10] Schnell, A., Vorberg, D., Ketzmerick, R. & Eckardt, A. High-temperature nonequilibrium bose condensation induced by a hot needle. *Phys. Rev. Lett.* **119**, 140602 (2017).

[11] Mullin, W. J. Bose-einstein condensation in a harmonic potential. *Journal of Low Temperature Physics* **106**, 615–641 (1997).

[12] Kirton, P. & Keeling, J. Thermalization and breakdown of thermalization in photon condensates. *Phys. Rev. A* **91**, 033826 (2015).

[13] Björk, G., Karlsson, A. & Yamamoto, Y. Definition of a laser threshold. *Phys. Rev. A* **50**, 1675–1680 (1994).

[14] Moodie, R. I., Kirton, P. & Keeling, J. Polarization dynamics in a photon bose-einstein condensate. *Phys. Rev. A* **96**, 043844 (2017).

[15] Greveling, S., van der Laan, F., Jagers, H. & van Oosten, D. Polarization of a bose-einstein condensate of photons in a dye-filled microcavity. *arXiv preprint arXiv:1712.08426* (2017).

[16] Schmitt, J. *et al.* Observation of Grand-Canonical Number Statistics in a Photon Bose-Einstein Condensate. *Phys. Rev. Lett.* **112**, 030401 (2014).

[17] Marelic, J. *et al.* Spatiotemporal coherence of non-equilibrium multimode photon condensates. *New J. Phys.* **18**, 103012 (2016).